Anomalous dispersion via dissipative coupling in a quantum well exciton-polariton microcavity

D. Biegańska,[1,*] M. Pieczarka,[1] C. Schneider,[2] S. Höfling,[3] S. Klembt,[3] and M. Syperek[1]

[1] *Department of Experimental Physics, Faculty of Fundamental Problems of Technology, Wrocław University of Science and Technology, Wybrzeże Wyspiańskiego 27, 50-370 Wrocław, Poland*

[2] *Carl von Ossietzky Universität Oldenburg, Fakultät V, Institut für Physik, 26129 Oldenburg, Germany*

[3] *Julius-Maximilians-Universität Würzburg, Physikalisches Institut and Würzburg-Dresden Cluster of Excellence ct.qmat, Lehrstuhl für Technische Physik, Am Hubland, 97074 Würzburg, Germany*

According to the principles of quantum mechanics the Hamiltonian describing a closed system's energies must be Hermitian. This leads to an avoided crossing on resonance, as coupling between states causes the energy levels to repel. This concept lies at the heart of exciton-polariton physics, where coherent exciton-photon interaction causes polariton branches to repel in momentum dispersion. However, non-Hermitian physics predicts an opposite effect: level attraction, which occurs when significant energy dissipation is present in the system. Here, we show a manifestation of dissipative coupling in a high-quality AlGaAs-based polariton microcavity, where two polariton branches attract, resulting in an anomalous, inverted dispersion of the lower branch in momentum dispersion. We observe the evolution of the level attraction with exciton-photon detuning, leading to changes in anomalous dispersion shape within a single sample. The dissipative coupling is explained by the interaction with an indirect exciton, acting as a highly dissipative channel in our system, and the observed dispersions are well captured within a phenomenological model. Our results present a new mechanism of dissipative coupling in light-matter systems and offer a tunable and well-controlled AlGaAs-based platform for engineering the non-Hermitian and negative mass effects in polariton systems.

INTRODUCTION

In interacting quantum systems it is typical to observe level repulsion. When two modes couple and intermix, the resulting energy levels anticross, avoiding degeneracy at resonance. If the strongly interacting states are photons in planar microvavities, and excitons confined in the medium inside the optical cavity, the resulting eigenstates appear as two exciton-polariton branches. Lower polaritons are characterized by a nearly parabolic dispersion at small wavevectors, which curvature is directly linked to their effective mass, inherited largely from the photonic component. At larger momenta charachteristic inflection points appear, around which the second derivative of the energy dispersion changes sign, nevertheless, the mass that determinines the group velocity remains positive for all momenta. In case the strong coupling is lost, the eigenstate dispersions become trivial, with parabolic modes and positive effective mass in the whole momentum domain. In any case, the mode dispersion and particle effective mass can be further engineered, e.g. by introducing an additional potential landscape in the system, such as lattice potentials, yet it requires additional sample processing or sophisticated excitation schemes [1–3].

However, in all open systems, losses are inevitable, and the level interactions and emerging eigenstates are strongly affected by the dissipation. Optical system in which light confinement can be effectively engineered, such as high-quality optical microcavities, are an ideal experimental platform to study dissipation-related coupling effects. When dissipation becomes equally important as the coherent coupling, emergent states can attract (instead of repelling), even without additional potential. The attraction effect is analogous to classical in-phase oscillations of dissipatively coupled pendulums [4]. In light-matter systems the influence of dissipative coupling has been experimentally observed in photonic-crystal cavities containing single quantum dots [5]. In two-dimensional polaritonic systems however, while there were some first experimental hints in rather low-Q microcavities containing monolayer semiconductors [6, 7], clear studies in low-linewidth systems are elusive so far. The phenomenon has mainly been studied in other contexts, such as magnons [4, 8, 9], microwave cavities [10] or mechanical systems [11]. Dissipative coupling has also been suggested as a potential mechanism for entangled state creation, as a new tool in the design of superconducting qubits [8, 9], for development of metamaterials [8], but also as the mechanism crucial in cavity spintronics [9]. As losses and dissipation are ubiquitous to praclically all physical systems, it influences any coherently coupled system.

When levels with parabolic dispersions are being subject to substantial loss, but the interlevel coupling and energy proximity are both sufficient, they attract, and the dispersion of one of the appearing modes can invert, presenting anomalous behaviour. The resulted band has a negative curvature parabolic wavevector dependence, directly representing the negative effective mass of the emergent quasiparticle. Furthermore, the negative mass manifests itself in the particle's dynamics, so that

* dabrowka.bieganska@pwr.edu.pl

its group velocity and momentum have opposing directions. Next to substantial fundamental interest, this, in turn, can be employed to control the wavepacket dynamics [12], hydrodynamics [13], or cause resonance trapping [14]. Negative mass can also be used in a wide range of studies on non-Hermitian effects or topology [15–17]. For those applications, engineering the inverted dispersion is crucial, yet so far cavity engineering focused mainly on the potential engineering or spin-orbit interactions in polariton microcavities, rather than the dissipation. Precise control over the attraction strength would also be hugely beneficial.

In exciton-polariton settings anomalous dispersion has been predicted [18], but it has been experimentally observed only very recently and only in transition-metal dichalcogenide samples [6, 7]. This medium lacks the exciton energy control and ease of the cavity design of a III-V based semiconductor and proved to be challenging in reproducibility. Moreover, in the observations made so far, the effect was strongly obscured by inhomogeneously broadened lines, while their theoretical descriptions vary widely.

In this work, we unequivocally demonstrate the level attraction manifested as an inverted anomalous dispersion in the AlGaAs exciton-polariton system. We investigate the mechanism of dissipation in our structure, crucial for the attraction to occur. In contrast to previous studies, our III-V semiconductor sample not only hosts conventionally studied Γ-excitons in the QWs, coherently coupled to photons, but also lower-energy spatially- and momentum-indirect X-excitons, which are strongly prone to dissipation. We show that the source of dissipation in our structure is the lower-energy indirect state, acting as a draining channel for both photons and electrons. This highly dissipative mode allows for the lossy coupling to become sufficiently strong to surpass the inherent exciton-photon coupling, and result in inverted eigenstate dispersion. Finally, we demonstrate the superiority of our material system in comparison to previous realisations, owing to its high tunability, ease of design and huge potential for non-Hermitian phases engineering.

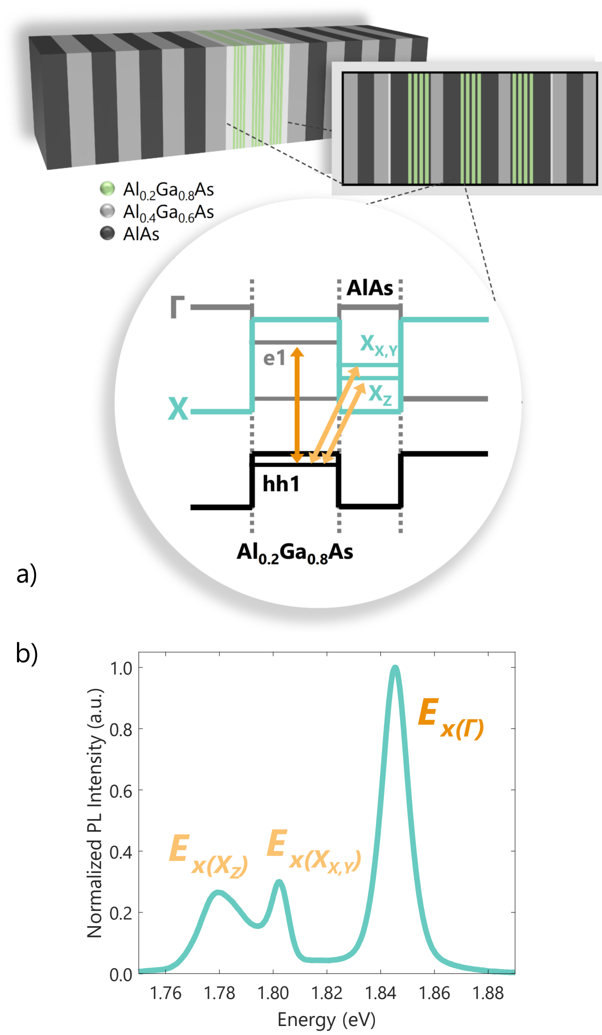

Figure 1. The investigated structure. (a) Schematics of the investigated microcavity, with a close-up of the active layer. In the system band structure solid lines show the edges of the X, Γ and valence bands of one period of the repeated layers. Dashed lines indicate the quantized electron ($e1$, $X_{X,Y}$, X_Z) and heavy hole ($hh1$) levels in two adjacent layers. Carriers occupying these levels subsequently form three excitons present within the system (indicated with orange arrows), when subject to Coulomb interactions. (b) The photoluminescence spectrum of the bare quantum well system, with the top Bragg reflector etched away. Three well-resolved features, labeled as $E_{x(\Gamma)}$, $E_{x(X_{X,Y})}$ and $E_{x(X_Z)}$, correspond to transitions of three excitonic species present in our sample.

RESULTS

Excitonic structure

We studied an AlGaAs/AlAs optical microcavity, designed for room temperature polaritonics [19]. However, in this work we focus on experimental observations made at cryogenic temperature of 4 K, benefitting from the excellent polaritonic linewidths. The sample schematic is depicted in Fig. 1(a), and the detailed description of the sample composition can be found in Methods.

Due to the high aluminium content the structure hosts both direct and indirect excitons in the quantum well (QW) layers [19, 20]. Apart from the conventional direct excitons composed of Γ-valley electrons and heavy holes confined in the QW layer (in type-I arrangement), the structure hosts also lower-energy spatially and momentum indirect X-excitons [21]. As the X-valley energy minimum is located above the Γ point energy for the $Al_{0.2}Ga_{0.8}As$ material in the QW, but it is reverse in the AlAs in the barrier, the QW band alignment for electrons in the X-valley is of the type-II. This results in quantum confinement of electron states in the barrier and allows the formation of indirect excitons composed of X-valley electrons in the barrier layer Coulomb-correlated with Γ-valley heavy holes confined in the QW layer. Two lowest-energy optically active states relate to excitons consisting of X-valley electrons with different effective masses (longitudinal and transverse with respect to the spatial quantization axis), forming X_Z and $X_{X,Y}$ states respectively. The single-particle energy levels are visualized in the active layers band structure in Fig. 1(a), using dashed lines. Spectrum of the bare QW active material is presented in 1(b), where all excitonic transitions are indicated. The indirect nature of these excitonic states as well as their transport properties has been investigated in our previous work [21].

When embedded in a monolithic optical microcavity close to resonance with the Γ-state, direct excitons couple strongly to light, forming exciton-polariton quasi-particles [19] (see also Supplementary Material). These states are characterized by the normal-mode splitting of $\hbar\Omega_\Gamma \approx 12meV$. However, herein we study the structure at very large negative Γ-exciton − photon detunings, $\Delta_\Gamma = E_c - E_{x(\Gamma)} < 0$ (where E_c is the cavity mode energy and $E_{x(\Gamma)}$ is the energy of the direct exciton in the QW). In this region the light-matter interactions are dominated by the coupling of the cavity optical mode to the indirect X -valley excitons and the resulting states strongly differ from the typical exciton-polariton curves under coherent light-matter coupling [22]. The detuning is sufficiently large that the coherent coupling to the Γ-excitons becomes irrelevant, i.e. $|\Delta_\Gamma| \gg \hbar\Omega_\Gamma$. For convenience, throughout the rest of the paper, we will refer to the detuning as defined with respect to the higher energy X-exciton, $\Delta_X = E_c - E_{x(X_{X,Y})}$.

Photoluminescence Measurements

To characterize the system and study the coupling between photons and X-excitons, we measured angle-resolved photoluminescence spectra in a wide detuning range, close to the resonance with the X-excitons. When the photonic mode gets sufficiently close to the energy of the $X_{X,Y}$ excitonic resonance, a new lower energy state brightens up, with the dispersion curved in a distinctly inverted manner. An experimental example of such a momentum dispersion is presented in Fig. 2(a), together with the extracted peak energies of the two branches. A very clear and monotonous redshift of this mode's energy with increasing wavevector can be seen in Fig. 2(b), a dependence opposite to the higher energy photonic state. The two levels clearly attract, causing the mirroring of their wavevector energy dispersions. Such an inverted-parabola curvature is directly linked to the negative effective mass of the lower mode and is a rare phenomenon in exciton-polariton systems[6, 7, 23, 24].

Taking advantage of the cavity energy gradient (due to the thickness variation across the sample), we probed the negative mass states in a range of sample positions (detunings). As presented in Fig. 2(c), decreasing the detuning between the cavity mode and the $X_{X,Y}$-exciton energy leads to an increase in attraction effect, with the anomalous shape of the lower branch becoming steeper and more distinct. Fig. 2(c) shows the energies of two polaritonic branches extracted from the PL measurements taken at different sample positions. Interestingly, around the positive photon to $X_{X,Y}$-exciton detuning of approximately 10 meV the curvature changes from the inverted parabola-like with one energy maximum at $k = 0$ to anomalous shape with two distinct and symmetric maxima at $k \neq 0$. Similar dispersion shapes have been observed before in different structures in both regimes [6, 7], yet never in the same material system, nor in a single sample.

At negative Δ_X detunings, when the cavity photon energy becomes lower than the $X_{X,Y}$-exciton, only one branch appears in the photoluminescence spectrum, with the standard parabolic shape of the dispersion resembling the one of a photonic mode, as presented in the Supplementary Material. For further discussions we focus on the level attraction region.

Model

In order to understand the source of level attraction, we have to recall the existence of the second excitonic resonance, X_Z-electron exciton, with energy below both the $X_{X,Y}$ resonance and the photonic mode, which inclusion is crucial in the theoretical description of the data. To correctly describe our system and quantify the mechanism of level attraction, we used a general three coupled oscillator model, predicting the attractive level crossing via the existence of a dissipative mode [25]. Such level attraction has been observed before, e.g. in magnonic systems [4, 8, 26–28]. The model can be described by a 3 x 3 non-Hermitian matrix:

$$
\begin{aligned}
H &= \begin{pmatrix} E_1 & V & g_1 \\ V & E_2 & g_2 \\ g_1 & g_2 & E_0 \end{pmatrix} \\
&= \begin{pmatrix} E_c - i\gamma_c & V & g_1 \\ V & E_{x(X_{X,Y})} - i\gamma_x & g_2 \\ g_1 & g_2 & E_{x(X_Z)} - i\gamma_0 \end{pmatrix}.
\end{aligned}
$$

In this approach two oscillators with intrinsic decay (with energies of E_1 and E_2) are coupled to each other coherently via V, and to the third oscillator E_0, which is strongly damped. Much larger dissipation of this third state is crucial for the level attraction and E_0's strong influence on the E_1 and E_2 dispersions, when the real coupling terms g_1 and g_2 are sufficiently large to surpass the inherent coupling V. In such conditions these terms can effectively act as complex coupling between the two modes [7, 8, 25], provided that E_1 and E_2 are nearly resonant. In a regime of high coherent coupling between

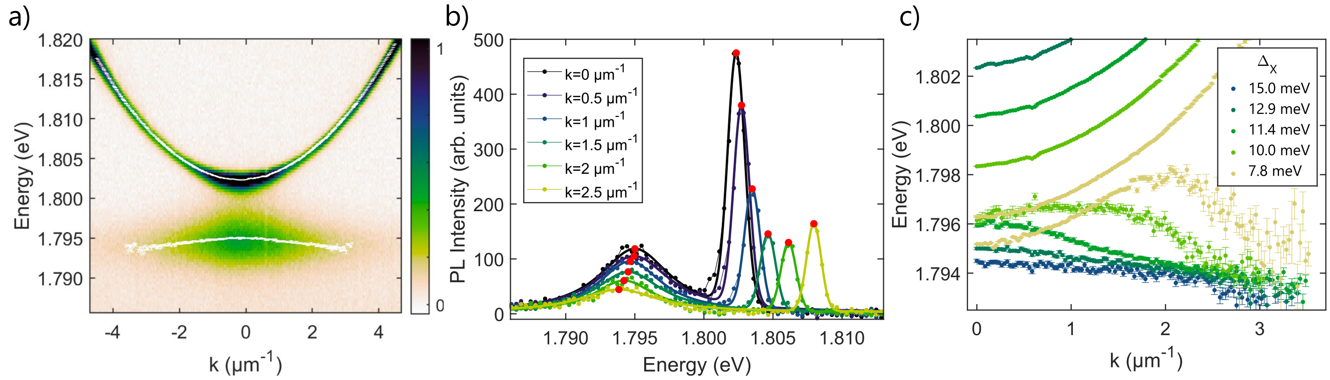

Figure 2. Experimental observation of the anomalous dispersion. (a) Momentum-resolved photoluminescence image at a chosen exciton-photon detuning. Spectra crossections taken at several wavevectors are presented in (b) (connected dots), together with fitted curves (solid lines). Red dots show the positions of extracted peaks of two branches, also marked in white in (a). (c) Extracted mode dispersions at several exciton-photon detunings Δ_X. Error bars indicate the fitting standard error.

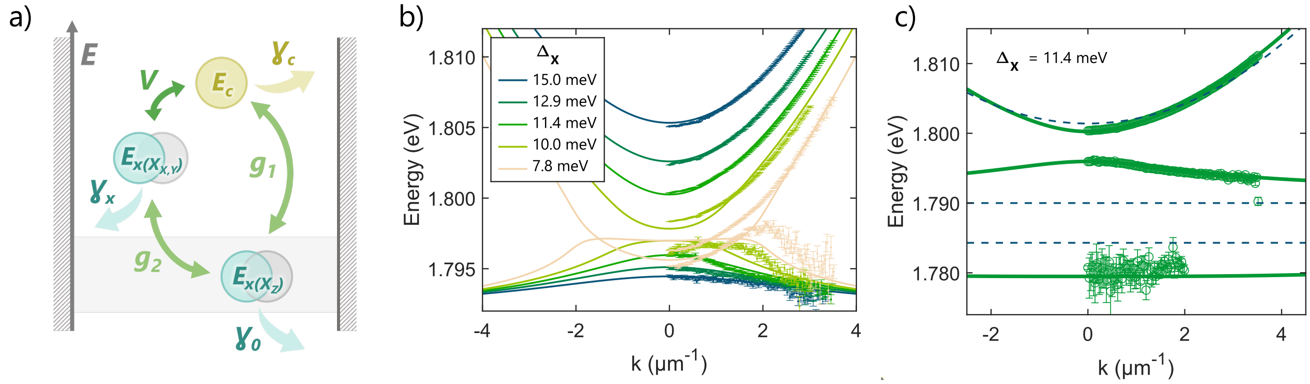

Figure 3. Level attraction modelling. (a) Schematic visualisation of the three coupled oscillators model and its use in our system. The coupled particles (photon (E_c) and two indirect excitons ($E_{x(X_{X,Y})}$ and $E_{x(X_Z)}$)) – are shown on the energy scale, with their intrinsic decays sketched as broad arrows, while the couplings are presented as two-sided arrows. (b) Comparison of the model lines with experimental level branches at several exciton-photon detunings, plotted in corresponding colors. Model parameters are described in the main text. (c) Example dispersion at a single photon-$X_{X,Y}$-exciton detuning of 11.4 meV. Dashed lines mark the dispersions of a bare photonic mode and two indirect excitons, open points are the fitted peak positions of the three polaritonic branches, and solid green lines are the model dispersions. For clarity, the experimental data is only presented for positive k.

the two resonances and a weak dissipation of the third mode all eigenstates repel, as it is typically observed in exciton-polariton systems [22, 29–32].

We schematically visualise the model and the involved oscillators in Fig. 3(a). In our structure, two coupled resonances are the photonic mode C and the $X_{X,Y}$ exciton, with energies and decay rates of E_c, $E_{x(X_{X,Y})}$ and γ_c, γ_x respectively. The lower-energy X_Z excitonic resonance (the ground state of the QW system) acts as a dissipative mode and is characterized by the energy of $E_{x(X_Z)}$ and dissipation γ_0. Coupling constant V describes the coupling between photons and $X_{X,Y}$ excitons inside the microcavity, which is expected to be weak, due to the space- and momentum- indirect nature of the excitonic resonance. On the contrary, X_Z-exciton is expected to couple to light more efficiently, as the spatial symmetry breaking allows for its recombination without the assistance of phonons, due to the weakening of the momentum-conservation rules, regardless of its indirect nature [21, 33, 34]. The coupling between the two indirect excitons is enabled via transfer of electrons between the states and transitions from the higher $X_{X,Y}$ to the lower X_Z electronic state, as evidenced by complex temporal dynamics [21] and previous studies [35–38]. Both couplings g_1 and g_2 are therefore expected to play a significant role in the system, with a g_1 value expected to be much larger than V. Energies of both excitonic resonances can be directly inferred from the photoluminescence measurements of the bare QW structure (see Fig. 1(b) and [21]).

Using this approach, we modelled our experimental dispersions as presented in Figs. 3(b) and (c). Experimental points are the extracted peak energies of the two polaritonic branches at several exciton-photon detunings Δ_X, and solid lines show the fitted model eigenstates. Additionally, in Fig. 3(c) we mark the dispersions of a bare photonic mode and two indirect excitons (dashed lines) at the exciton-photon detuning of 11.4 meV, as well as the extracted energies of the lowest-lying observed state (points).

Model results show very good correspondence with the measured dispersions. The model reflects well the anomalous shape of the lower branch dispersion and captures a clear transition between its monotonic (with a single maximum at $k = 0$) and non-monotonic (with maxima at finite wavevectors) $|k|$-dependence when decreasing Δ_X. At larger detunings the model dispersions match experimental points nearly perfectly, demonstrating the change in curvature around $k = 0$, linked to the dissipative level attraction. Discrepancies between the model and the experimental curves become visible only at smaller positive exciton-photon detunings ($\Delta_X \leq 10$ meV). However, we highlight the fact, that to model our data we set all the parameters constant throughout this detuning range, which is a simplified approach. We focus mainly on the regime where dissipative coupling results in a negative effective mass with a distinct maximum at $k = 0$, where the model correctly reproduces the experimental results. The transition featuring a maximum at finite k is not fully captured, as the model simplifies here. All three decay constants, as well as level energies, can vary across the sample, due to the local disorder and the layer width change. Nevertheless, the model describes our system very well in a large range of exciton-photon detunings, even when using only one set of parameters.

The extracted exciton-photon couplings are $V = 0.1$ meV and $g_1 = 10.6$ meV, while the coupling between two X-excitons g_2 is 17 meV. As expected, the coherent coupling between the photonic mode and the spatially and momentum indirect $X_{X,Y}$ exciton is much smaller than other energies in our system. The highly dissipative X_Z state couples to light more efficiently, what is likely a result of the symmetry breaking effect described above. The most influential interaction comes from the nonradiative coupling between the two X-excitons. The extracted decay rates of all states are $\gamma_c = 0.1$ meV, $\gamma_x = 0.01$ meV and $\gamma_0 = 41$ meV. The model photon linewidth value corresponds to a lifetime of approximately ~ 6 ps, which is a value expected for this microcavity, subject to disorder and operating far from the optimal parameter range (with a large detuning from the designed wavelength) [39]. A very small broadening of the $X_{X,Y}$ state points to its longer lifetime, resulting from its indirect nature. On the other hand, large inherent broadening γ_0 of the X_Z exciton points to its dissipative role and it is crucial to obtain level attraction in our system. We note that the model value is larger than the measured photoluminescence linewidth broadening of this state of ~ 20 meV, measured with the top mirror removed from the cavity [21]. However, the observed emission linewidth cannot be directly translated into the inherent damping and homogenous broadening. Photoluminescence broadening consists of both homogeneous and inhomogeneous parts, but, at the same time, can be narrowed by a very low Q-factor microcavity formation and subsequent Purcell effect [22]. Large damping of this mode can result from its ground state nature, making the X_Z excitons more prone to structure inhomogeneities and affecting their lifetime and transport properties, as shown before [21, 40]. Overall, the model accurately describes our system and reveals the highly damped X_Z excitons as the source of the level attraction and inverted polariton dispersion.

In addition, we considered the contribution of the three involved oscillators in the final system eigenvalues, by studying the Hopfield coefficients [41, 42]. Coefficient dispersions reflect the anomalous behaviour of the inverted anomalous branch, with the dissipative exciton fraction gaining importance in the anomalous region (at small wavevectors), especially at small detunings. It further highlights the importance of the X_Z excitons in the observed effect. Hopfield dispersions at two different detunings ($\Delta_X = 11.4$ meV and $\Delta_X = 7.8$ meV, corresponding to two aforementioned regimes of the anomalous branch dispersion), as well as their more detailed discussion, can be found in the Supplementary Material.

DISCUSSION

In summary, we have observed the anomalous dispersion of the polaritonic branch in an AlGaAs-based microcavity, characterized by the state's negative effective mass. Our system uniquely allows to taylor the coherent coupling and the optical Q-factor as well as the dissipation by engineering the $X_{X,Y}$ and X_Z exciton. It has been shown before how dissipative form of coupling between excitons and photons can lead to such dispersion, while the exact mechanism of this coupling can vary from interactions between room temperature excitons and phonons [7], coupling of both excitons and photons to the same decay channel [14, 18], or to a third dissipative mode [25]. In this work, we have shown how the presence and coupling to the indirect excitonic state energetically below the excitonic and photonic resonances, which acts as a channel of loss, can manifest itself as a dissipative coupling between these states. High dissipation rate of this mode is crucial to make the effective coupling non-Hermitian and overcome the coherent coupling. Furthermore, we have observed the evolution of the system eigenstates with varying detuning, showing the shift and the change of eigenstate dispersion curvature. We show two regimes of anomalous dispersion shape, with eigenstate energy maxima at $k = 0$ and $k \neq 0$ in a single sample. Our hypothesis is supported by a phenomenological model of three coupled oscillators.

It is important to note that the anomalous dispersion has been observed before in exciton-polariton systems, yet so far only in transition metal dichalcogenide-based samples. First observation [6] was reported for trion-polaritons in $MoSe_2$ and its supporting model is applicable only for many-particle excitons in heavily-doped samples, with complex interactions. Subsequent observation [7] showed the negative-mass exciton-polaritons in the WS_2 monolayer in optical microcavities with different exciton-photon detunings. The observation was made at room temperature and the suggested mechanism of dissipative coupling in this system is via exciton-phonon interactions, supported by a microscopic theory. In our case of a III-V semiconductor-based system at cryogenic temperature, phonon influence is known to be much smaller, hence insufficient to lead to the dissipative coupling. Previously studied systems lacked the presence of a tuneable and energetically-lower state providing a channel of loss, which proves to be crucial in our structure. They also lacked the excellent linewidths, making the dispersion shape less distinct and rendering interpretations of the observed dispersions less robust.

Recent theoretical studies have also investigated the effect of non-Hermitian coupling in exciton-polariton systems, both in lossy optical microcavities [18] and for 2D-layer polaritons without the microcavity [43], showing an increasing interest in this field and more universal behaviour of lossy systems. Apart from exciton-polariton studies, level attraction has been studied also in other systems, such as magnon, optomechanical, or microwave cavities [4, 5, 8, 10, 11, 14, 26–28, 44, 45]. In each of these cases dissipation is an essential component in the finding, even though the exact mechanism of dissipative coupling or the interacting particles differ. Macroscopic models proved to be applicable in different scenarios [4, 14, 25].

Most importantly, our system provides a great opportunity for level attraction strength tuning, via changing the detuning between the resonances. Subsequent change of the eigenstate dispersion curvature, hence the particle effective mass, can be easily tuned by simply changing the position on the sample, owing to its wedged growth. Such easy tuning and effective mass engineering was lacking in previous observations and shows a clear path for future designs. Anomalous dispersion can be employed in novel studies of non-Hermitian effects [15, 16, 46], nontrivial dynamics and hydrodynamics [12, 47] and in studies of analogue systems [48–50].

Moreover, the AlGaAs-based microcavity is superior to previously reported TMDcs in linewidths, reproducibility, and control during growth, further enhancing its huge potential for design. This work paves the way for future studies on non-Hermitian dispersion engineering. It also allows access to plethora of studies on the exceptional points and related phenomena, such as winding of the complex eigenenergies, chiral modes, topological lasing, or enhanced perturbation, among others [17, 51–53].

METHODS

Sample

The sample under study consists of twelve 9 nm-wide $Al_{0.20}Ga_{0.80}As$ QWs, separated by 4 nm AlAs barriers, distributed in three stacks of four (as visualized in Fig. 1). The stacks are placed in a $\lambda/2$-AlAs cavity surrounded by AlAs/$Al_{0.40}Ga_{0.60}As$ distributed Bragg reflectors (DBRs), consisting of 28/24 mirror pairs in the bottom/top reflector, including 3 nm GaAs smoothing layers after each mirror pair in the local minimum of the electromagnetic field. Whole microcavity structure was grown by molecular beam epitaxy on the GaAs substrate. Lack of the wafer rotation during growth results in a gradual change of the cavity length across the sample, allowing for the experimental access to a wide range of exciton-photon detunings. The photoluminescence spectrum of the bare quantum well system presented in Fig. 1(b) was taken on a sample with the top Bragg reflector etched away [21].

Optical Measurements

The sample was placed in the continuous flow liquid helium cryostat and cooled down to 4.2 K. It was excited by laser pulses from the OPO pumped by a Ti:Sapphire pulsed laser with 76 MHz repetition rate, generating the wavelength of around 620 nm. The beam was focused on a sample via a NA = 0.65 objective. Structure photoluminescence was then collected by the same objective and imaged on a slit of a monochromator (with a 1200 lines/cm groove density diffraction grating) equipped with a high-efficiency EMCCD camera. Imaging the Fourier plane by using four confocal lenses in the detection path allowed for the angle-resolved measurements.

Dispersion extraction

Photoluminescence spectra at each wavevector were fitted with a sum of a Lorentzian (lower central energy) and Gaussian (higher energy) curves. The extracted peak energies were used for further modelling. The error bars presented throughout the manuscript come from the fitting standard error.

DATA AVAILABILITY

The datasets generated during and/or analysed during the current study are available from the corresponding author on reasonable request.

[1] C. Schneider, K. Winkler, M. D. Fraser, M. Kamp, Y. Yamamoto, E. A. Ostrovskaya, and S. Höfling, Reports on Progress in Physics **80**, 016503 (2016).
[2] D. Tanese, H. Flayac, D. Solnyshkov, A. Amo, A. Lemaître, E. Galopin, R. Braive, P. Senellart, I. Sagnes, G. Malpuech, and J. Bloch, Nature Communications **4**, 1749 (2013).
[3] C. E. Whittaker, E. Cancellieri, P. M. Walker, D. R. Gulevich, H. Schomerus, D. Vaitiekus, B. Royall, D. M. Whittaker, E. Clarke, I. V. Iorsh, I. A. Shelykh, M. S. Skolnick, and D. N. Krizhanovskii, Phys. Rev. Lett. **120**, 097401 (2018).
[4] M. Harder, B. M. Yao, Y. S. Gui, and C.-M. Hu, Journal of Applied Physics **129**, 201101 (2021).
[5] T. Tawara, H. Kamada, T. Tanabe, T. Sogawa, H. Okamoto, P. Yao, P. K. Pathak, and S. Hughes, Opt. Express **18**, 2719 (2010).
[6] S. Dhara, C. Chakraborty, K. M. Goodfellow, L. Qiu, T. A. O'Loughlin, G. W. Wicks, S. Bhattacharjee, and A. N. Vamivakas, Nature Physics **14**, 130 (2018).
[7] M. Wurdack, T. Yun, M. Katzer, A. G. Truscott, A. Knorr, M. Selig, E. A. Ostrovskaya, and E. Estrecho, Nature Communications **14**, 1026 (2023).
[8] M. Harder, Y. Yang, B. M. Yao, C. H. Yu, J. W. Rao, Y. S. Gui, R. L. Stamps, and C.-M. Hu, Phys. Rev. Lett. **121**, 137203 (2018).
[9] Y.-P. Wang and C.-M. Hu, Journal of Applied Physics **127**, 130901 (2020).
[10] V. L. Grigoryan, K. Shen, and K. Xia, Phys. Rev. B **98**, 024406 (2018).
[11] F. Elste, S. M. Girvin, and A. A. Clerk, Phys. Rev. Lett. **102**, 207209 (2009).
[12] D. Colas, F. P. Laussy, and M. J. Davis, Physical Review Letters **121**, 055302 (2018), arXiv:1801.04779.
[13] D. Ballarini, D. Caputo, C. S. Muñoz, M. De Giorgi, L. Dominici, M. H. Szymańska, K. West, L. N. Pfeiffer, G. Gigli, F. P. Laussy, and D. Sanvitto, Phys. Rev. Lett. **118**, 215301 (2017).
[14] E. Persson, I. Rotter, H.-J. Stöckmann, and M. Barth, Phys. Rev. Lett. **85**, 2478 (2000).
[15] M. Parto, Y. G. N. Liu, B. Bahari, M. Khajavikhan, and D. N. Christodoulides, Nanophotonics **10**, 403 (2021).
[16] T. Gao, E. Estrecho, K. Y. Bliokh, T. C. H. Liew, M. D. Fraser, S. Brodbeck, M. Kamp, C. Schneider, S. Höfling, Y. Yamamoto, F. Nori, Y. S. Kivshar, A. G. Truscott, R. G. Dall, and E. A. Ostrovskaya, Nature **526**, 554 (2015).
[17] T. Long, X. Ma, J. Ren, F. Li, Q. Liao, S. Schumacher, G. Malpuech, D. Solnyshkov, and H. Fu, Advanced Science **9**, 2203588 (2022).
[18] O. Bleu, K. Choo, J. Levinsen, and M. M. Parish, Phys. Rev. A **109**, 023707 (2024).
[19] H. Suchomel, S. Kreutzer, M. Jörg, S. Brodbeck, M. Pieczarka, S. Betzold, C. P. Dietrich, G. Sęk, C. Schneider, and S. Höfling, Opt. Express **25**, 24816 (2017).
[20] N. Chand, T. Henderson, J. Klem, W. T. Masselink, R. Fischer, Y.-C. Chang, and H. Morkoĉ, Physical Review B **30**, 4481 (1984).
[21] D. Biegańska, M. Pieczarka, K. Ryczko, M. Kubisa, S. Klembt, S. Höfling, C. Schneider, and M. Syperek, Optical properties and dynamics of direct and spatially and momentum indirect excitons in algaas/alas quantum wells (2024), arXiv:2404.01938 [cond-mat.mes-hall].
[22] A. V. Kavokin, J. Baumberg, G. Malpuech, and F. Laussy, *Microcavities*, 1st ed. (Oxford University Press, Oxford, 2008).
[23] D. Colas and F. P. Laussy, Phys. Rev. Lett. **116**, 026401 (2016).
[24] E. Y. Paik, L. Zhang, S. Hou, H. Zhao, Y. Chou, S. R. Forrest, and H. Deng, Advanced Optical Materials **11**, 2201440 (2023).
[25] W. Yu, J. Wang, H. Y. Yuan, and J. Xiao, Phys. Rev. Lett. **123**, 227201 (2019).
[26] I. Boventer, C. Dörflinger, T. Wolz, R. Macêdo, R. Lebrun, M. Kläui, and M. Weides, Phys. Rev. Res. **2**, 013154 (2020).
[27] B. Yao, T. Yu, X. Zhang, W. Lu, Y. Gui, C.-M. Hu, and Y. M. Blanter, Phys. Rev. B **100**, 214426 (2019).
[28] B. Bhoi, B. Kim, S.-H. Jang, J. Kim, J. Yang, Y.-J. Cho, and S.-K. Kim, Phys. Rev. B **99**, 134426 (2019).
[29] M. Wurdack, N. Lundt, M. Klaas, V. Baumann, A. V. Kavokin, S. Höfling, and C. Schneider, Nature Communications **8**, 259 (2017).
[30] O. Koksal, M. Jung, C. Manolatou, A. N. Vamivakas, G. Shvets, and F. Rana, Phys. Rev. Res. **3**, 033064 (2021).
[31] Y. V. Zhumagulov, S. Chiavazzo, D. R. Gulevich, V. Perebeinos, I. A. Shelykh, and O. Kyriienko, npj Computational Materials **8**, 92 (2022).
[32] M. Höfner, S. Sadofev, B. Kobin, S. Hecht, and F. Henneberger, Applied Physics Letters **107**, 181109 (2015).
[33] B. Pietka, *Excitonic Complexes in Natural Quantum Dots Formed in Type II GaAs / AlAs*, Ph.D. thesis, Université Joseph-Fourier - Grenoble I (2007).
[34] G. Danan, B. Etienne, F. Mollot, R. Planel, A. M. Jean-Louis, F. Alexandre, B. Jusserand, G. Le Roux, J. Y. Marzin, H. Savary, and B. Sermage, Physical Review B **35**, 6207 (1987).
[35] J. Feldmann, M. Preis, E. Göbel, P. Dawson, C. Foxon, and I. Galbraith, Solid State Communications **83**, 245 (1992).
[36] E. Finkman, M. Sturge, M.-H. Meynadier, R. Nahory, M. Tamargo, D. Hwang, and C. Chang, Journal of Luminescence **39**, 57 (1987).
[37] A. Wysmołek, B. Chwalisz, M. Potemski, R. Stępniewski, A. Babiński, S. Raymond, and V. Thierry-Mieg, Acta Physica Polonica A **106**, 367 (2004).
[38] G. Peter, E. Göbel, W. Rühle, J. Nagle, and K. Ploog, Superlattices and Microstructures **5**, 197 (1989).
[39] G. Panzarini, L. C. Andreani, A. Armitage, D. Baxter, M. S. Skolnick, V. N. Astratov, J. S. Roberts, A. V. Kavokin, M. R. Vladimirova, and M. A. Kaliteevski, Physics of the Solid State **41**, 1223 (1999).
[40] S. T. Lee, J. Haetty, A. Petrou, P. Hawrylak, M. Dutta, J. Pamulapati, P. G. Newman, and M. Taysing-Lara, Phys. Rev. B **53**, 12912 (1996).
[41] M. I. Vasilevskiy, D. G. Santiago-Pérez, C. Trallero-Giner, N. M. R. Peres, and A. Kavokin, Phys. Rev. B **92**, 245435 (2015).
[42] J. J. Hopfield, Phys. Rev. **112**, 1555 (1958).

[43] R. Binder, J. R. Schaibley, and N. H. Kwong, Phys. Rev. B **109**, 125301 (2024).
[44] J. Okołowicz, M. Płoszajczak, and I. Rotter, Physics Reports **374**, 271 (2003).
[45] Y. Yang, J. Rao, Y. Gui, B. Yao, W. Lu, and C.-M. Hu, Phys. Rev. Appl. **11**, 054023 (2019).
[46] L. Feng, R. El-Ganainy, and L. Ge, Nature Photonics **11**, 752 (2017).
[47] M. A. Khamehchi, K. Hossain, M. E. Mossman, Y. Zhang, T. Busch, M. M. Forbes, and P. Engels, Phys. Rev. Lett. **118**, 155301 (2017).
[48] L. Pickup, H. Sigurdsson, J. Ruostekoski, and P. G. Lagoudakis, Nature Communications **11**, 4431 (2020).
[49] M. J. Jacquet, T. Boulier, F. Claude, A. Maître, E. Cancellieri, C. Adrados, A. Amo, S. Pigeon, Q. Glorieux, A. Bramati, and E. Giacobino, Philosophical Transactions of the Royal Society A: Mathematical, Physical and Engineering Sciences **378**, 20190225 (2020).
[50] P. St-Jean, A. Dauphin, P. Massignan, B. Real, O. Jamadi, M. Milicevic, A. Lemaître, A. Harouri, L. Le Gratiet, I. Sagnes, S. Ravets, J. Bloch, and A. Amo, Phys. Rev. Lett. **126**, 127403 (2021).
[51] R. Su, E. Estrecho, D. Biegańska, Y. Huang, M. Wurdack, M. Pieczarka, A. G. Truscott, T. C. H. Liew, E. A. Ostrovskaya, and Q. Xiong, Science Advances **7**, eabj8905 (2021).
[52] F. Baboux, D. D. Bernardis, V. Goblot, V. N. Gladilin, C. Gomez, E. Galopin, L. L. Gratiet, A. Lemaître, I. Sagnes, I. Carusotto, M. Wouters, A. Amo, and J. Bloch, Optica **5**, 1163 (2018).
[53] V. Ardizzone, F. Riminucci, S. Zanotti, A. Gianfrate, M. Efthymiou-Tsironi, D. G. Suàrez-Forero, F. Todisco, M. De Giorgi, D. Trypogeorgos, G. Gigli, K. Baldwin, L. Pfeiffer, D. Ballarini, H. S. Nguyen, D. Gerace, and D. Sanvitto, Nature **605**, 447 (2022).

ACKNOWLEDGEMENTS

D. B., M.P. and M. S. acknowledge financial support from the National Science Centre Poland within the Grant No. 2018/30/E/ST7/00648. C.S. and S.K. gratefully acknowledge funding by the German Research Association (DFG) within the project SCHN1376 13.1 and KL 3124/3-1 (El Pollo Loco). S.H. and S.K. acknowledge financial support by the DFG under Germany's Excellence Strategy - EXC2147 ct.qmat (Project No. 390 858 490). S.H. acknowledges financial support by the DFG project HO 5194/12-1.

AUTHOR CONTRIBUTIONS STATEMENT

D. B. conducted all the spectroscopic experiments and analysed the experimental data. D.B. and M.P. performed theoretical modeling of the results. S. K., S. H, and C. S provided the sample. D.B., M.P., M.S. analyzed the results and all authors contributed to their discussion. D.B. wrote the first version of the manuscript and prepared all figures. All authors reviewed the manuscript to its final form.

ADDITIONAL INFORMATION

The authors declare no competing interests. Supplementary Information is available for this paper.